Advanced Optical Materials

Coupling and Interlayer Exciton in Twist-Stacked WS2 Bilayers

--Manuscript Draft--

Manuscript Number:	
Full Title:	Coupling and Interlayer Exciton in Twist-Stacked WS2 Bilayers
Article Type:	Full Paper
Section/Category:	
Keywords:	Transition metal dichalcogenides; 2D materials; interlayer coupling; interlayer exciton
Corresponding Author:	Hong Jin Fan Nanyang Technological University Singapore, SINGAPORE
Corresponding Author Secondary Information:	
Corresponding Author's Institution:	Nanyang Technological University
Corresponding Author's Secondary Institution:	
First Author:	Shoujun Zheng
First Author Secondary Information:	
Order of Authors:	Shoujun Zheng
	Linfeng Sun
	Xiaohao Zhou
	Fucai Liu
	Zheng Liu
	Zexiang Shen
	Hong Jin Fan
Order of Authors Secondary Information:	
Abstract:	Interlayer electronic and mechanical couplings of transitional metal dichalcogenides (TMDs) due to Van der Waals force determine their band structure and Raman modes evolution, respectively. We have synthesized twist-stacked WS2 bilayers with twist angles of 0°, 13°, 30°, 41°, 60°, and 83° via chemical-vapor deposited, which allows us to study the coupling effect by Raman and photoluminescence spectroscopy and density function calculation. The photoluminescence property implies that these random-twisted WS2 bilayers behave as quasi-direct bandgap material due to weakened interlayer coupling as a result of larger interlayer distances than the non-twisted 0° and 60° stacked WS2 bilayers (with an indirect band gap). In addition, an additional small peak (AI) near the excitonic transition peak (A) is observed from the twisted bilayers, which can be attributed to the interlayer exciton transition.
Additional Information:	
Question	**Response**
Please submit a plain text version of your cover letter here. Please note, if you are submitting a revision of your manuscript, there is an opportunity for you to provide your responses to the reviewers later; please do not add them to the cover letter.	Dear Editor, We are pleased to submit our manuscript for publication consideration in Advanced Optical Materials. All authors have read and approved this manuscript. The work reported here is original and unpublished. This Interlayer coupling in 2D materials are interesting because it determines many physical properties. Typical 2D materials (MoS2, WS2, etc) bilayers are generally indirect bandgap materials showing weak photoluminescence (PL). Herein we

	synthesized a series of twist-stacked WS2 bilayers, and established that the twisting with non-regular angles causes weakened inter-layer coupling and new inteer-layer excitons. This is very interesting result and may stimulate new thinking on how to manipulate the electronic and optical properties of bilayers by adjusting the stacking angles. Sincerely, Prof. Hong Jin Fan School of Physical and Mathematical Sciences Nanyang Technological University, Singapore E-mail: fanhj@ntu.edu.sg URL: www.ntu.edu.sg/home/fanhj

WILEY-VCH

DOI: 10.1002/ ((please add manuscript number))
Article type: Full paper

Coupling and Interlayer Exciton in Twist-Stacked WS_2 Bilayers

*Shoujun Zheng, Linfeng Sun, Xiaohao Zhou, Fucai Liu, Zheng Liu, Zexiang Shen, Hong Jin Fan**

S. Zheng, Prof. Z. X. Shen, Prof. H. J. Fan
Centre for Disruptive Photonic Technologies, Nanyang Technological University, 637371, Singapore
E-mail: fanhj@ntu.edu.sg

S. Zheng, L. Sun, Prof. Z. X. Shen, Prof. H. J. Fan
Division of Physics and Applied Physics, School of Physical and Mathematical Sciences, Nanyang Technological University, 637371, Singapore

Dr. X. Zhou
National Laboratory for Infrared Physics, Shanghai Institute of Technical Physics, Chinese Academy of Sciences, Shanghai 200083, China

Dr. F. Liu, Prof. Z. Liu
School of Materials Science and Engineering, Nanyang Technological University, 639798, Singapore

Keywords: Transition metal dichalcogenides, 2D materials, interlayer coupling, interlayer exciton

Interlayer electronic and mechanical couplings of transitional metal dichalcogenides (TMDs) due to Van der Waals force determine their band structure and Raman modes evolution, respectively. We have synthesized twist-stacked WS_2 bilayers with twist angles of 0°, 13°, 30°, 41°, 60°, and 83° via chemical-vapor deposited, which allows us to study the coupling effect by Raman and photoluminescence spectroscopy and density function calculation. The photoluminescence property implies that these random-twisted WS_2 bilayers behave as quasi-direct bandgap material due to weakened interlayer coupling as a result of larger interlayer distances than the non-twisted 0° and 60° stacked WS_2 bilayers (with an indirect band gap). In addition, an additional small peak (A_I) near the excitonic transition peak (A) is observed from the twisted bilayers, which can be attributed to the interlayer exciton transition.

1. Introduction

Van der Vaals interaction between atomic layers in two-dimensional (2-D) materials affects their physical properties such as evolution of band structure from indirect band gap (bulk) to direct band gap (monolayer) in MoS_2.[1] Vertical twisted 2-D materials are good platforms to study Van de Waals coupling, such as twisted graphene bilayer,[2-5] transitional metal dichalcogenides (TMDs) bilayer,[6] and vertical heterostructures.[7, 8] Some interesting phenomena were reported in twisted graphene bilayers such as Van Hove singularities,[9] Dirac electrons localization,[4] and Hofstadter's butterfly.[10, 11] In vertical stacked MoS_2/WS_2 heterostructure which was fabricated by transferring MoS_2 flakes to WS_2 flakes, a new photoluminescence (PL) peak emerged after annealing in vacuum which is dictated by charge transfer and band normalization between the WS_2 and MoS_2 layers.[12] Also, indirect band gap peak of 15° twisted MoS_2 grown by chemical vapor deposition (CVD) method has a smaller redshift due to the larger interlayer distance compared to the ones of AA and AB stacked MoS_2.[13] Although WS_2 has a similar atomic structure to MoS_2, very different properties have been shown, such as larger valence band splitting of WS_2 (0.41eV)[14] than MoS_2 (0.16eV).[1, 15] Also, the degree of circular polarization of A exciton emission under near-resonant excitation is around 95% in WS_2 bilayer[16] in contrast to 10–30% in MoS_2 bilayer.[17]

In this letter, we demonstrate the observation of WS_2 bilayers and trilayers with various twist angles on quartz plates by CVD method. The twisted bilayers have much intensive PL compared to both monolayers and untwisted bilayers (AA and AB stackings) and the absence of indirect transition peak. This implies that the random twisted WS_2 bilayer possesses a quasi-direct band gap behavior as a result of weakened coupling due to enlarged interlayer distance.

2. Experimental results

Our samples were growth by CVD method at 1100°C using the setup shown in **Figure 1**a. A magnet was applied to push the sulfur source in the furnace (see details in method). Bilayer WS_2 with twist angles of 0°, 13°, 30°, 41°, 60°, and 83° were observed from one experiment

and on the same substrate as shown in Figure 1b-g. The twist angle is defined by rotation of upper layer related to the lower layer at counter-clockwise direction. We can see that the smaller upper monolayer WS_2 triangle is twisted to different angles in related to the bigger lower monolayer WS_2 in each sample.

Monolayer WS_2 is a direct band gap material whereas WS_2 bilayers with AA or AB stacking is known to have an indirect band gap due to the interlayer electronic coupling.[18, 19] However, as the symmetry between upper and lower layer is broken, the random twisted WS_2 bilayer samples are expected to have interlayer distance and degree of coupling different from the AA-stacked (0° twist) WS_2 bilayer. Photoluminescence can provide useful information on the bandgap structure and direct or indirect bandgap transition. **Figure 2**a shows the PL spectra of the twisted WS_2 bilayers. PL spectra of the WS_2 bilayer with 0° and 60° twist angle (viz., AA and AB stacking) show two dominating peaks that correspond to direct transition peak A and indirect transition peak I. This is well within expectation and proves that the 0° and 60° twisted WS_2 bilayers are indirect band gap materials. However, for the random twisted WS_2 bilayers (13°, 30°, 41°, and 83°) the PL spectra are very different. Firstly, the PL intensity is much stronger than that of AA or AB stacked bilayer. For example, PL intensity of 30° twisted WS_2 bilayer is about 22 times stronger than the 0° sample. Secondly, the indirect transition peak I seen in the AA or AB stacked bilayers is absent in random twisted bilayers. Thirdly, a small peak A_I shows up in the PL spectra of random twisted bilayers. All these PL features indicate prove that the random twisted WS_2 bilayer has a different band structure from AA or AB stacking WS_2 bilayers. To show clearly the changes of PL spectra, we fit the PL curves by Lorentz function and plot as a function of the twisting angle in Figure 2b. As can be seen, the PL curves in random twisted WS_2 bilayers are composed of three peaks (peak A, peak A_I, and peak I). Note that Peak A and peak A_I are also observed in the absorbance spectrum in Figure 2c. Peak I is absent in the absorbance spectrum, which corroborates the assignment of indirect transitions.

Phonon vibrations in 2-D TMDs are very sensitive to interlayer coupling and are useful in identifying the layer number of TMDs.[20] We also investigated Raman spectra of our samples in Figure 2d. The out-of-plane vibration mode A_{1g} of the random twisted bilayers both redshifts and broadens with respect to the 0° and 60° bilayers. The longitudinal acoustic phonon (2LA) blueshifts in random twisted bilayers. The in-plane mode E^1_{2g} which is merged into the 2LA mode peak may have the same trend with 2LA. The broadening and redshift of A_{1g} mode in random twisted WS_2 bilayers has a similar trend with the monolayer WS_2, which proves that interlayer mechanical coupling of random twisted bilayers is weaker than the AA or AB stacked bilayers.

To further verify our results, we also measured the PL spectra of our samples at excitation wavelength of 457 nm. The result is presented in **Figure 3**a. Similar to the result by 532 nm excitation, PL spectra of the random twisted WS_2 bilayers show that there bilayers are quasi-direct band gap materials. Both Raman modes of E^1_{2g} and A_{1g} can be seen in Figure 3b since the 2LA mode becomes much weaker at 457 nm excitation. We can clearly see that E^1_{2g} of random twisted bilayers blueshifts compared to the ones of 0° and 60° bilayers. This can be more clearly seen from the summary of both peak shift and Raman intensity ratio of E^1_{2g} to A_{1g} modes in Figure 3c. The peak difference, $\omega(A_{1g})-\omega(E^1_{2g})$, of the random twisted bilayer is smaller than the AA or AB stacked bilayer. Also, the intensity ratio of two modes in the random twisted bilayer is near to that of monolayer, which implies that the mechanical coupling in the random twisted bilayer is weaker than that of AA or AB ones.

In addition to twisted bilayers, twisted trilayer WS_2 were also observed with twist angle of 30°, 0°, and 60° (see **Figure 4**a-c). In this case, the bottom layer has an AA stacking configuration on top of which a new layer grow with twisted symmetry. PL spectra of the trilayer WS_2 are shown in Figure 4d. Different from twisted bilayer WS_2, trilayer WS_2 with 30° twisted angle does have a strong indirect peak I which is also blueshifted with respect to the

ones of 0° and 60° twist angles. Interestingly, the new peak A_I also appears at slightly higher energy position than peak A, which is similar to the case of twisted bilayers. Again, this new peak was also observed in the absorbance spectrum of 30° twisted trilayer (see inset in Figure 4d), indicative of its excitonic nature. Raman spectra of twisted trilayer are shown in Figure 4e. As expected, the E^1_{2g} mode of 30° twisted trialyer has a weaker Raman intensity than the ones of 0° and 60°. Peak positions of both E^1_{2g} and A_{1g} modes have no obvious shift in the twisted trilayers.

3. Calculation

In order to understand the coupling evolution of twisted WS_2 bilayer, we conducted *ab initio* calculations on the band structure and interlayer distance at different twist angels. The result is plotted in **Figure 5**. The values do not exactly match experiment data, because partially of the diffeent twist angles used in the ideal atomic model; Neverthelss, we are more interested in the trend. The interlayer distance is about 0.627 nm of 27.8° twisted WS_2 bilayers which is larger than the ones of AA (0.593 nm) and AB (0.595 nm) stacking configurations. The increased interlayer distance of random twisted bilayers, which is due to the steric repulsion effect[13], may explain the broadening and redshift of A_{1g} modes in Figure 2d. In addition, Figure 5 also shows that the random twisted bilayers have an evidently larger indirect band gap than AA or AB stacked one. For example, the indirect band gap of 27.8° twisted bilayer increased by 0.35 eV compared to the AA stacked one. Such a larger blueshift may clarify the PL spectra of our samples in Figure 2a. Fitting of the PL curve show that the indirect peak (1.83 eV) of 30° twisted bilayer has a 0.15 eV blueshift compared to the one (1.70 eV) of AA stacking bilayer (see **Figure 6**a). Both the enlarged interlayer distance and blueshift of indirect band gap prove the weakened interlayer couplings in random twisted bilayers, which are manifested by their extraordinary PL spectra.

4. Discussion

Twisted TMDs bilayer is good platform to study many-body phenomenon, such as interlayer exciton[6, 21] and trion.[22] Due to the spin and layer pseudospin coupling in TMDs AB stacking bilayer, interlayer hopping energy is twice of spin-orbital coupling (SOC) strength.[16, 22] In other words, interlayer hopping is greatly suppressed due to spin-layer locking effect. However, the larger interlayer distance and symmetry breaking in the random twisted WS_2 bilayer make interlayer hopping possible to form an interlayer exciton. The PL peak fitting of 30° twisted WS_2 bilayer is shown in **Figure 6**a. The peak A_I (1.98 eV) is supposed to result from the interlayer exciton transition and peak A (1.90 eV) from the well-known intralayer excitonic transition. Both peaks are clearly observed in the absorbance spectra, which implies that these two peaks originates from excitonic transitions. Figure 6b illustrates the interlayer exciton and intralayer exciton in the twisted WS_2 bilayer, in which the binding energy of interlayer exciton is lower than that of intralayer one.[23-25] The binding energy of interlayer exciton A_I is about 80 meV less than the one of intralayer exciton A ($E_{AI} - E_A$ = 1.98 eV –1.9 eV). In this random twisted bilayer, the weaker interlayer coupling allows carrier to transfer from one layer to the other and form interlayer electron-hole pairs.

Conclusion

WS_2 bilayers with different twist angles have been grown by CVD method at high temperature (1100 °C) and are employed for the study of interlayer coupling. It is found that these random twisted WS_2 bilayers possess a quasi-direct band gap PL characteristics with much higher intensity than the non-twisted AA or AB stacked bilayers(e.g., 22 times stronger at 30° stacking compared to 0° one). This extraordinary PL results from weakened interlayer coupling between the twisted bilayers due to increased interlayer distance. Calculation reveals that random twisted bilayers have larger interlayer distance and blueshift of indirect transition energy compared to AA or AB stacked bilayer. In addition to the A excitonic transition peak, another peak A_I has been observed in PL spectra of both random twisted bilayers and trilayers. We attribute this peak A_I to the interlayer excitonic transition. These random twisted WS_2

bilayers with adjustable interlayer coupling could be a suitable platform to investigate optoelectronic and spin-valley properties.

Experimental Section

CVD growth of twisted WS_2 bilayer: Our samples were grown on quartz plates by CVD method as in Figure 1a. Quartz plate was covered on the top of a sapphire boat which was placed in a 25 mm diameter quartz tube and put at the center of furnace. WO_3 powder as a precursor was spread on a piece of Si wafer and put on the bottom of the sapphire boat. Another precursor 0.1 g sulfur powder was put in a quartz boat and placed on the outside of furnace. The furnace was flowed by 200 sccm pure Ar for 30 min then 20 sccm Ar when furnace started heating. The furnace was heated up to 1100 °C at the rate of 20 °C/min. When temperature reached to 1100 °C, sulfur powder was pushed to the edge of the furnace so that sulfur powder became melting and supplied S vapor to the center of the furnace. After 20 min growth, the furnace cool down naturally. Growth process is at atmospheric pressure.

Optical characterization: Optical images are taken on Nikon microscope with a 100× objective lens. PL at 532 nm and 457 nm excitation wavelength is conducted on a WITEC CRM200 Raman system with 150 line mm^{-1} grating. Raman mapping at excitation wavelength of 457 nm is measured on a WITEC CRM200 Raman system with 1800 line mm^{-1} grating. Raman spectra at 532 nm is measured on a Renishaw Invia Raman microscope. Absorbance spectra is measured on JASCO Microspectrophotometer with a 5 □m spot size.

Calculation method: Our calculations were based on density functional theory (DFT) within the local density approximation formulated by Perdew and Wang (PWC)[26] as implemented in the DMol^3 code.[27, 28] Because the weak interactions are not well described by the standard exchange-correlation functional, the DFT-D (D stands for dispersion) approach within the OBS scheme was adopted for the vdW corrections.[29] DFT Semi-core Pseudopots (DSPP), which induce some degree of relativistic correction into the core, were used for the core treatment.

Moreover, double numerical atomic orbital plus polarization was chosen as the basis set, with the global orbital cutoff of 4.6 Å. The k-point was set to 9 × 9 ×1 for the structural optimization and 15 × 15 × 1 for the electronic properties calculations, and the smearing value was 0.005 Ha (1 Ha = 27.2114 eV). The convergence tolerance of energy, maximum force, and maximum displacement were set to 1.0 105 Ha, 0.002 Ha Å, and 0.005 Å, respectively. A large vacuum of 30 Å was used to prevent the interaction and artificial dipole moment effects from neighboring cells in the direction normal to the WS_2 surface.

Acknowledgement This work is supported by Singapore Ministry of Education Academic Research Fund Tier 3 (Grant No. MOE2011-T3-1-005). S. Zheng and L. Sun contributed equally to this work.

[1] K. F. Mak, C. Lee, J. Hone, J. Shan, T. F. Heinz, *Phys. Rev. Lett.* **2010**, 105, 136805.

[2] K. Kim, S. Coh, L. Z. Tan, W. Regan, J. M. Yuk, E. Chatterjee, M. F. Crommie, M. L. Cohen, S. G. Louie, A. Zettl, *Phys. Rev. Lett.* **2012**, 108, 246103.

[3] R. W. Havener, H. Zhuang, L. Brown, R. G. Hennig, J. Park, *Nano Lett.* **2012**, 12, 3162.

[4] G. Trambly de Laissardiere, D. Mayou, L. Magaud, *Nano Lett.* **2010**, 10, 804.

[5] A. K. Geim, I. V. Grigorieva, *Nature* **2013**, 499, 419.

[6] S. Huang, X. Ling, L. Liang, J. Kong, H. Terrones, V. Meunier, M. S. Dresselhaus, *Nano Lett.* **2014**, 14, 5500.

[7] Y. Gong, J. Lin, X. Wang, G. Shi, S. Lei, Z. Lin, X. Zou, G. Ye, R. Vajtai, B. I. Yakobson, H. Terrones, M. Terrones, B. K. Tay, J. Lou, S. T. Pantelides, Z. Liu, W. Zhou, P. M. Ajayan, *Nat. Mater.* **2014**, 13, 1135.

[8] X. Duan, C. Wang, J. C. Shaw, R. Cheng, Y. Chen, H. Li, X. Wu, Y. Tang, Q. Zhang, A. Pan, J. Jiang, R. Yu, Y. Huang, X. Duan, *Nat. Nanotechnol.* **2014**, 9, 1024.

[9] G. Li, A. Luican, J. L. Dos Santos, A. C. Neto, A. Reina, J. Kong, E. Andrei, *Nat. Phys.* **2010**, 6, 109.

[10] C. Dean, L. Wang, P. Maher, C. Forsythe, F. Ghahari, Y. Gao, J. Katoch, M. Ishigami, P. Moon, M. Koshino, *Nature* **2013**, 497, 598.

[11] B. Hunt, J. D. Sanchez-Yamagishi, A. F. Young, M. Yankowitz, B. J. LeRoy, K. Watanabe, T. Taniguchi, P. Moon, M. Koshino, P. Jarillo-Herrero, R. C. Ashoori, *Science* **2013**, 340, 1427.

[12] S. Tongay, W. Fan, J. Kang, J. Park, U. Koldemir, J. Suh, D. S. Narang, K. Liu, J. Ji, J. Li, R. Sinclair, J. Wu, *Nano Lett.* **2014**, 14, 3185.

[13] K. Liu, L. Zhang, T. Cao, C. Jin, D. Qiu, Q. Zhou, A. Zettl, P. Yang, S. G. Louie, F. Wang, *Nat. Commun.* **2014**, 5, 4966.

[14] H. R. Gutierrez, N. Perea-Lopez, A. L. Elias, A. Berkdemir, B. Wang, R. Lv, F. Lopez-Urias, V. H. Crespi, H. Terrones, M. Terrones, *Nano Lett.* **2013**, 13, 3447.

[15] A. Splendiani, L. Sun, Y. B. Zhang, T. S. Li, J. Kim, C. Y. Chim, G. Galli, F. Wang, *Nano Lett.* **2010**, 10, 1271.

[16] B. R. Zhu, H. L. Zeng, J. F. Dai, Z. R. Gong, X. D. Cui, *Proc. Natl. Acad. Sci. U.S.A.* **2014**, 111, 11606.

[17] S. F. Wu, J. S. Ross, G. B. Liu, G. Aivazian, A. Jones, Z. Y. Fei, W. G. Zhu, D. Xiao, W. Yao, D. Cobden, X. D. Xu, *Nat. Phys.* **2013**, 9, 149.

[18] W. Zhao, Z. Ghorannevis, L. Chu, M. Toh, C. Kloc, P. H. Tan, G. Eda, *ACS Nano* **2013**, 7, 791.

[19] W. Zhao, R. Ribeiro, M. Toh, A. Carvalho, C. Kloc, A. Castro Neto, G. Eda, *Nano Lett.* **2013**, 13, 5627.

[20] A. Berkdemir, H. R. Gutierrez, A. R. Botello-Mendez, N. Perea-Lopez, A. L. Elias, C. I. Chia, B. Wang, V. H. Crespi, F. Lopez-Urias, J. C. Charlier, H. Terrones, M. Terrones, *Sci. Rep.* **2013**, 3, 1755.

[21] T. Yu, M. Wu, *Phys. Rev. B* **2014**, 90, 035437.

[22] A. M. Jones, H. Yu, J. S. Ross, P. Klement, N. J. Ghimire, J. Yan, D. G. Mandrus, W. Yao, X. Xu, *Nat. Phys.* **2014**, 10, 130.

[23] P. Rivera, J. R. Schaibley, A. M. Jones, J. S. Ross, S. Wu, G. Aivazian, P. Klement, N. J. Ghimire, J. Yan, D. Mandrus, *Nat. Commun.* **2014**, 6, 6242.

[24] M.-H. Chiu, M.-Y. Li, W. Zhang, W.-T. Hsu, W.-H. Chang, M. Terrones, H. Terrones, L.-J. Li, *ACS Nano* **2014**, 8, 9649.

[25] P. Rivera, J. R. Schaibley, A. M. Jones, J. S. Ross, S. Wu, G. Aivazian, P. Klement, K. Seyler, G. Clark, N. J. Ghimire, J. Yan, D. G. Mandrus, W. Yao, X. Xu, *Nat. Commun.* **2015**, 6, 6242.

[26] J. P. Perdew, Y. Wang, *Phys. Rev. B: Condens. Matter* **1992**, 45, 13244.

[27] B. Delley, *J. Chem. Phys.* **1990**, 92, 508.

[28] B. Delley, *J. Chem. Phys.* **2000**, 113, 7756.

[29] F. Ortmann, F. Bechstedt, W. Schmidt, *Phys. Rev. B* **2006**, 73, 205101.

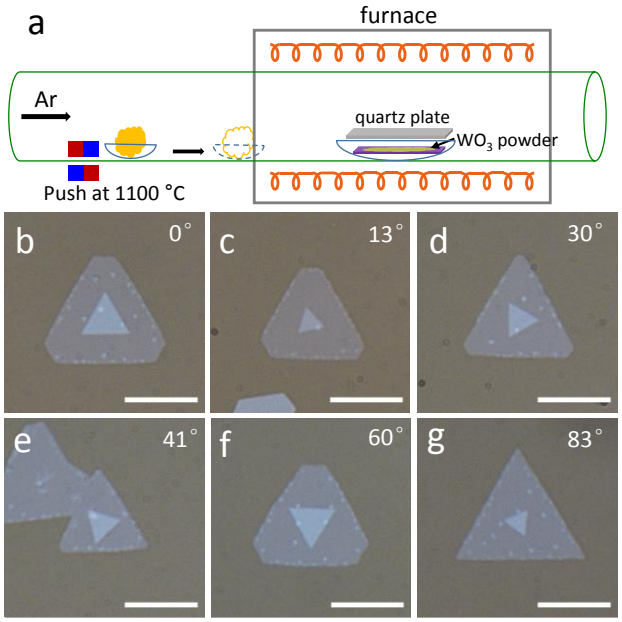

Figure 1. (a) CVD setup for the growth of WS_2 bilayers. (b)-(g) Optical images of the twisted WS_2 bilayers with twist angles of 0°, 13°, 30°, 41°, 60°, and 83°, respectively. The twist angle is defined by the rotation of top triangle with respect to the bottom one in counter-clockwise direction.

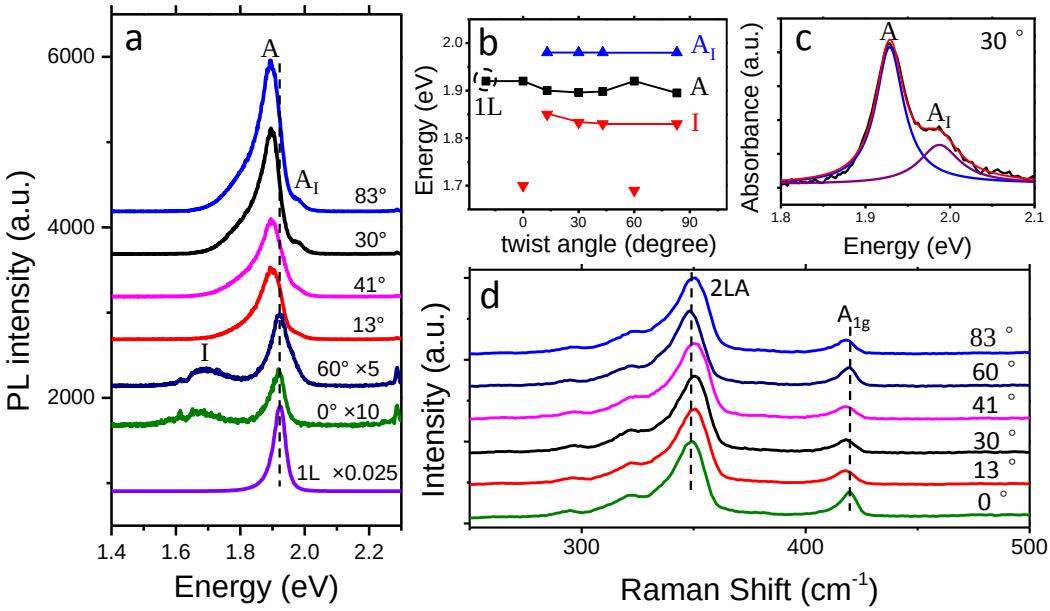

Figure 2. Photoluminescence and Raman results of twisted WS_2 bilayers at the excitation wavelength of 532 nm. (a) PL spectra of the random twisted WS_2 bilayers as a comparison to to the 0° and 60° twisted bilayers, and monolayer (1L). Note the stronger PL intensity of A exciton and disappearance of indirect transition peak I in the random twisted bilayers. (b) Summary of PL peaks position obtained by Lorentz fitting of the PL curves in (a). (c) Absorbance spectrum of the 30° twisted bilayer showing the peak A and A_I. (d) Raman spectra of all bilayer samples showing the redshift and broadening of the A_{1g} mode and blueshift of 2LA mode (E^1_{2g} mode is merged into 2LA).

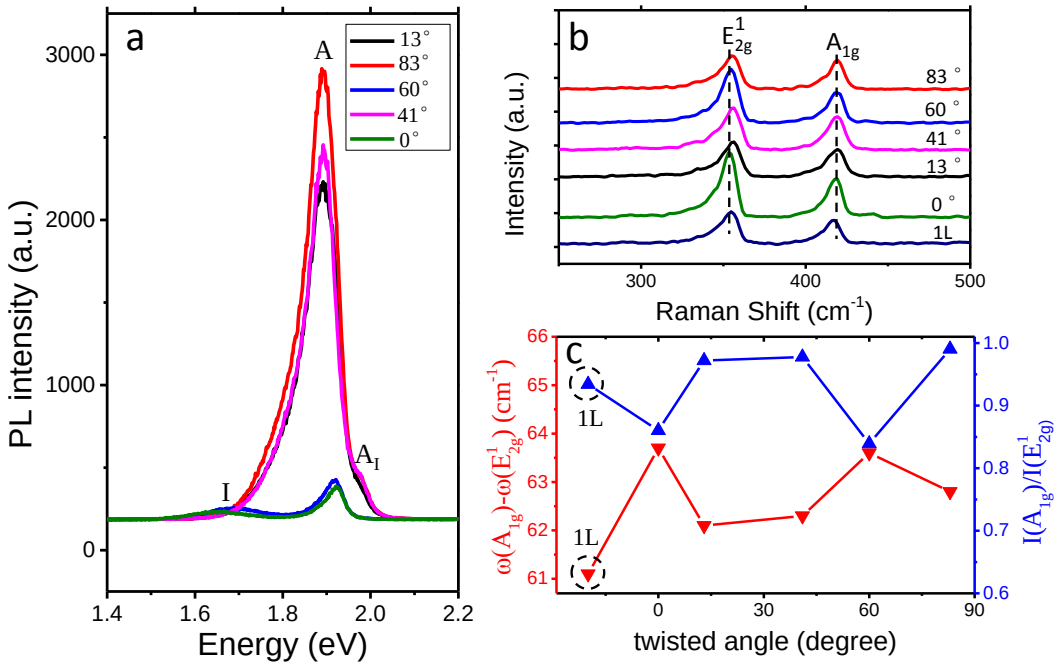

Figure 3. Photoluminescence and Raman results of twisted WS_2 bilayers at excitation wavelength of 457 nm. (a) PL spectra of the bilayers, showing the large intensity of peak A and absence of peak I in the random twisted bilayers. (b) Raman spectra. (c) Peak position difference and the intensity ratio of A_{1g} to E^1_{2g}. Data from monolayer (1L) is included.

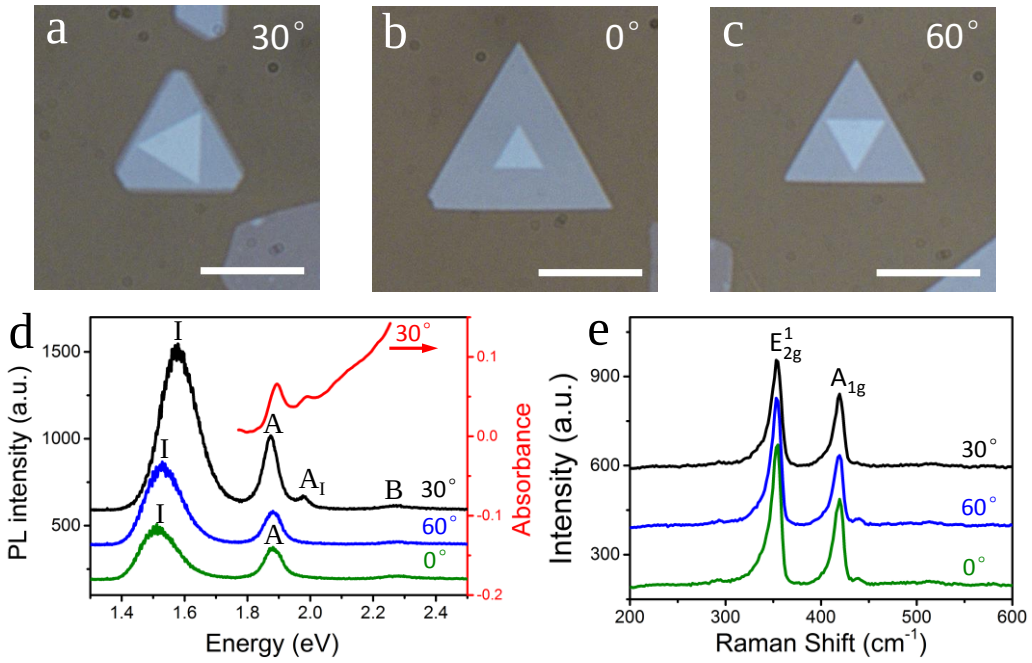

Figure 4. Optical images and PL spectra of twisted WS_2 trilayers at excitation wavelength of 457 nm. (a)-(c) Optical images of the trilayers with twist angle of 30°, 0°, and 60°. Scale bars are 10 μm. (d) PL spectra. A new peaks A_I presents in the 30° twisted trilayer. Red curve is the absorbance spectrum of 30° twisted trilayer in (a). (e) Raman spectra.

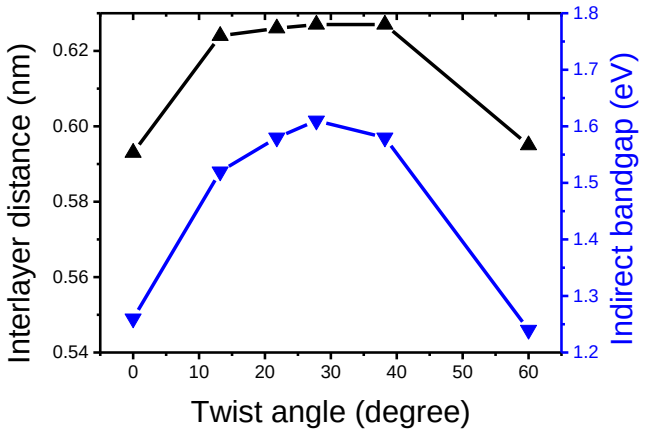

Figure 5 Calculated interlayer distance and indirect bandgap energy as a function of different twist angles in WS_2 bilayers.

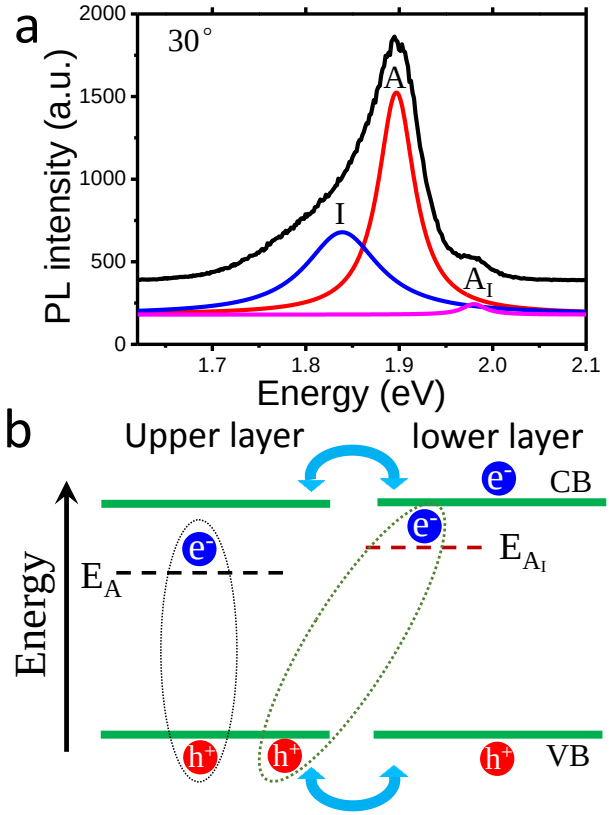

Figure 6 (a) Lorentz fitting of the PL spectra of the 30° twisted WS_2 bilayer (black line) showing the peak A, peak A_I, and peak I. (b) Schematics of intralayer exciton state and interlayer exciton state in the twisted WS_2 bilayer.